RESEARCH ARTICLE

ADVANCED PHYSICS RESEARCH Open Access

www.advphysicsres.com

A Near Room Temperature Curie Temperature in a New Type of Diluted Magnetic Semiconductor $(Ba,K)(Zn,Mn)_2As_2$

Yi Peng, Xiang Li, Luchuan Shi, Guoqiang Zhao, Jun Zhang, Jianfa Zhao, Xiancheng Wang, Bo Gu, Zheng Deng,* Yasutomo J. Uemura, and Changqing Jin**

Achieving room-temperature ferromagnetism is one of the major challenges for diluted magnetic semiconductors (DMS). $(Ba,K)(Zn,Mn)_2As_2$ (BZA) belongs to a new type of DMS materials that feature independent spin and carrier doping. In previous studies, BZA shows a reliable Curie temperature (T_C) of 230 K, a record among these types of materials. In this work, progress in further experimentally enhancing T_C of BZA to 260 K is reported by increasing Mn concentration with parallel K doping, as supported by complementary first-principles calculations. A sufficient carrier concentration can suppress the short-range antiferromagnetic interaction of the nearest Mn—Mn pair, which suppresses ferromagnetism in DMS materials. Consequently, a higher T_C has been obtained in BZA with improved Mn- and K-doping levels by using high-pressure synthesis that effectively eliminates structural distortion and overcomes the limitation of chemical solution in BZA. The work demonstrates an effective strategy to enhance T_C in DMS systems.

1. Introduction

Combining the features of carrier control in semiconductors and spin control in ferromagnets, diluted magnetic semiconductors (DMS) have significant advantages in spintronics and have thus been extensively studied in recent decades.[1–3] For example, spin-orbit torque, which was first discovered in DMS, is now an important mechanism for the new generation of magnetic memories and sensors.[4] In the 1990s, the typical DMS, (Ga,Mn)As, was successfully conducted spin and carrier doping via the substitution of Mn^{2+} into Ga^{3+} sites.[3,5] However, a single-element substitution such as this can lead to a lack of independent tuning for conducting or magnetic properties.[6,7] Furthermore, the dual roles of Mn complicate the underlying theoretical understanding, including whether double exchange is a relevant mechanism in these systems.[8] To overcome the aforementioned difficulties, a series of new type DMS materials with independent spin and carrier doping have been discovered, that is, Li(Zn,Mn)As and $(Ba,K)(Zn,Mn)_2As_2$ (BZA).[9–13] Among these new DMS materials, the reliable Curie temperature (T_C = 230 K) of BZA was the highest.[3,14,15]

Owing to the application potential of high-T_C BZA, it has been proposed to develop isostructural heterojunctions between BZA, superconducting $(Ba,K)Fe_2As_2$, and high Néel temperature semiconductor $BaMn_2As_2$ to explore their emerging phenomena and functionalities.[3,14,16] Particularly, their matching $ThCr_2Si_2$-type crystal structure and the small mismatch (less than 5%) within the a-b plane between them represent the unique features of BZA and analogs and could lead to unprecedented fabrications of potential heterojunctions for DMS materials, as shown in **Figure 1**. Taking the Andreev reflection junction as a typical example, the first theoretical consideration of the spin-flip Andreev reflection was studied with DMS, and recently it led to spin-triplet superconductivity at the interface of ferromagnet/superconductor.[17,18] Furthermore, the versatile design of materials properties, for example, superconductivity with ferromagnetism, topological magnetism, and enhanced spin–orbit couplings, could be accomplished via proximity effects.[19] These prospects have inspired further trials to improve T_C of BZA.[20–23] The intuitive way of improving T_C is to increase the doping level of magnetic cations in DMS materials.[16] For

Y. Peng, L. Shi, G. Zhao, J. Zhang, J. Zhao, X. Wang, Z. Deng, C. Jin
Institute of Physics
Chinese Academy of Sciences
Beijing 100190, China
E-mail: dengzheng@iphy.ac.cn; Jin@iphy.ac.cn

Y. Peng, L. Shi, G. Zhao, J. Zhang, J. Zhao, X. Wang, Z. Deng, C. Jin
School of Physics
University of Chinese Academy of Sciences
Beijing 101408, China

X. Li, B. Gu
Kavli Institute for Theoretical Sciences
University of Chinese Academy of Sciences
Beijing 100190, China
E-mail: gubo@ucas.ac.cn

Y. J. Uemura
Department of Physics
Columbia University
New York, NY 10027, USA

The ORCID identification number(s) for the author(s) of this article can be found under https://doi.org/10.1002/apxr.202400124

DOI: 10.1002/apxr.202400124

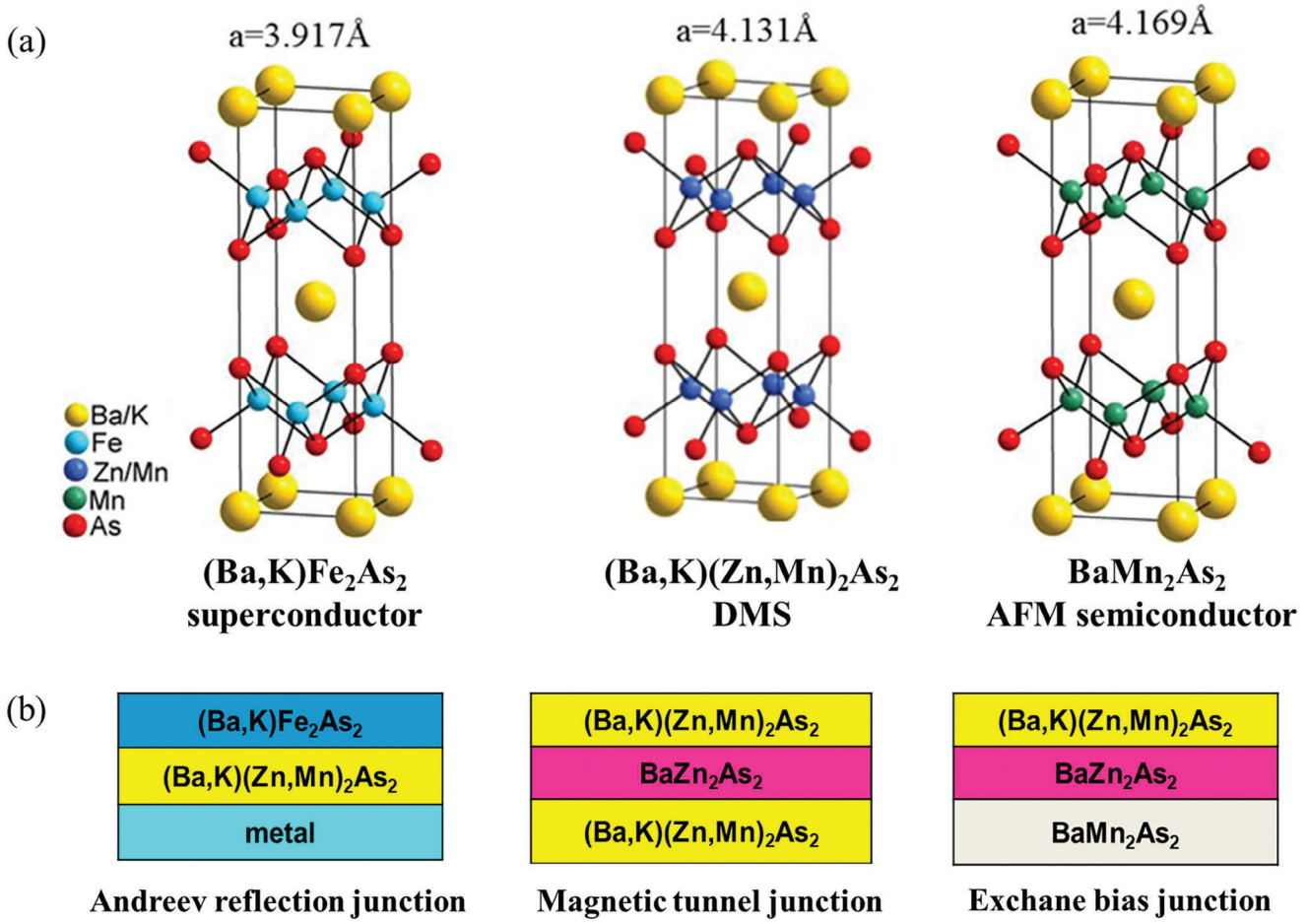

Figure 1. a) Crystal structures of BZA, $BaMn_2As_2$, and $(Ba,K)Fe_2As_2$. b) Proposed heterojunctions between the materials in Figure 1a.

example, T_C of (Ga,Mn)As has been enhanced to 200 K via heavy Mn doping.[24,25] It is worth noting that further Mn doping is a long-term challenge for (Ga,Mn)As, due to heterovalent (Ga^{3+}, Mn^{2+}) substitution. The latter results in not only limited chemical solubility but also interstitial Mn defects, which act as electron donors to balance hole carriers from substitutional Mn.[9,26] Such a disadvantage is overcome by isovalent (Zn^{2+}, Mn^{2+}) substitution in BZA. The Mn concentration over 15% is theoretically tolerable owing to the existence of isostructural $BaMn_2As_2$ with fully occupied Mn.[27]

It is well known that the magnetic exchange interaction between nearest Mn ions is antiferromagnetic superexchange, and it tends to dominate the interactions among all Mn ions and results in antiferromagnetism in DMS materials with increasing Mn-doping. Taking the advantage of independent spin and carrier doping, it is possible to study the individual doping effect on ferromagnetism. Our calculations indicate that carrier-doping, namely K-doping, can suppress the antiferromagnetic superexchange in BZA. Moreover, the sufficient carrier-doping can overcome the dominating antiferromagnetic interaction and further enhance T_C in heavy Mn-doped BZA. However, extra Mn doping has not been successful with conventional synthesis conditions. Generally, the doping levels in most of the DMS materials are limited due to either structural distortion or valence disequilibrium which can be induced by the impurity doping. High-pressure synthesis or annealing has shown the capability to recover structural distortions and maintain unstable valences in many materials.[28] With high-pressure and high-temperature annealing, the Mn concentration of BZA was increased to 28%, ≈2 times that of conventional synthesized samples. The high-pressure stabilized high doping levels in polycrystalline BZA finally led to the highest T_C of 260 K.

2. Results and Discussion

2.1. Crystal Structure

K and/or Mn-doped BZA samples crystalize into $ThCr_2Si_2$-type structure as shown in Figure 1a. In previous reports, Mn-related impurities formed when Mn doping level was over 15%.[8] Taking advantage of the high-pressure technique, higher concentrations of Mn can be stabilized in bulk BZA. The purity of all the samples $((Ba_{0.7}K_{0.3})(Zn_{1-x}Mn_x)_2As_2$ with $x = 0.18, 0.2, 0.22, 0.24, 0.26, 0.28$) was confirmed with powder X-ray diffraction (XRD) measurements. **Figure 2a** shows the XRD patterns and corresponding Rietveld refinement of $(Ba_{0.7}K_{0.3})(Zn_{0.76}Mn_{0.24})_2As_2$ as a typical example. All the Bragg peaks are indexed under the space group of I4/mmm, indicating the high purity of the

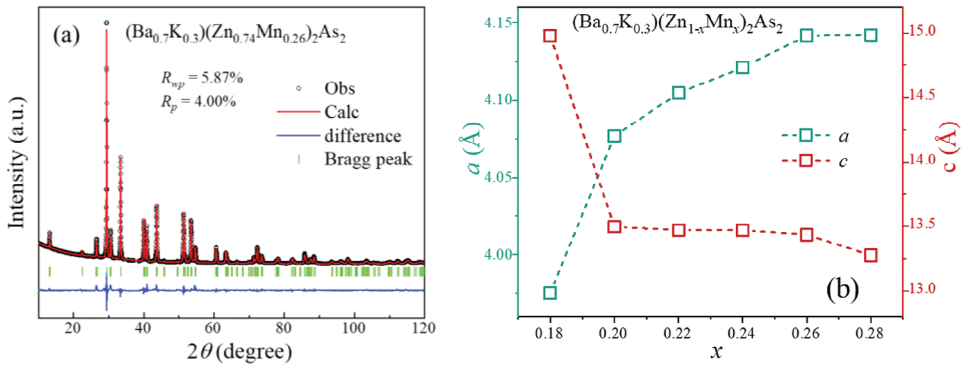

Figure 2. a) Powder X-ray diffraction pattern and refinement of $(Ba_{0.7}K_{0.3})(Zn_{1-x}Mn_x)_2As_2$. b) Lattice parameters of $(Ba_{0.7}K_{0.3})(Zn_{1-x}Mn_x)_2As_2$.

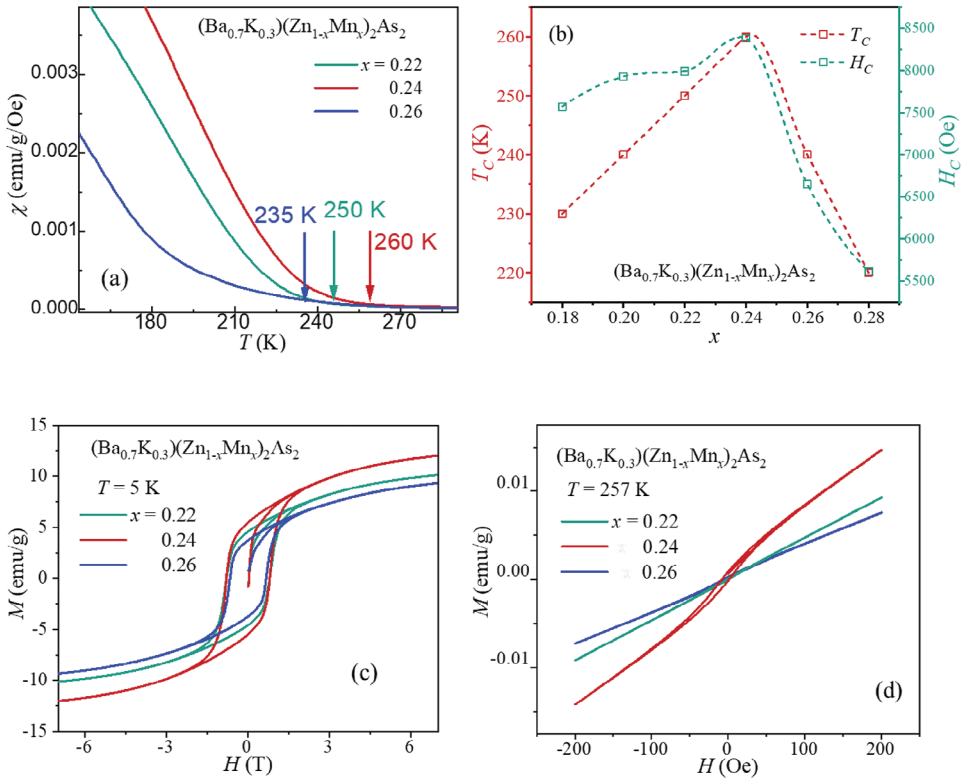

Figure 3. a) Temperature-dependent magnetization of $(Ba_{0.7}K_{0.3})(Zn_{1-x}Mn_x)_2As_2$ with $x = 0.22$, 0.24, and 0.26, in the vicinity of Curie temperatures. b) Curie temperatures and coercive forces versus Mn doping levels, x. c) Field-dependent magnetization of $(Ba_{0.7}K_{0.3})(Zn_{1-x}Mn_x)_2As_2$ with $x = 0.22$, 0.24, and 0.26 at 5 K. d) Field-dependent magnetization of $(Ba_{0.7}K_{0.3})(Zn_{1-x}Mn_x)_2As_2$ with $x = 0.22$, 0.24, and 0.26 at 257 K.

samples. Rietveld refinements were used to calculate the lattice parameters of samples. The dopant dependences of the lattice parameters, a and c, are shown in Figure 2b. We can see that the lattice parameters change monotonically with increasing Mn concentrations, suggesting successful chemical substitution.

2.2. Magnetic Properties

Temperature-dependent magnetization ($M(T)$) measurements were performed to determine T_C of the aforementioned samples. For the sake of simplification, $M(T)$ under the field cooling (FC) process for three selected samples are shown in **Figure 3a**. Similar to the previous report of BZA with lower doping levels, the upturns on the $M(T)$ curves, which indicate the forming of ferromagnetic ordering, are defined as T_C.[18] Figure 3b shows a clearly dome-shaped x dependence on T_C and coercive force (H_C). T_C increases with increasing Mn concentrations in the first place, and the highest $T_C = 260$ K is obtained in the sample with $(Ba_{0.7}K_{0.3})(Zn_{0.76}Mn_{0.24})_2As_2$. The overdoped Mn damages ferromagnetism due to the increased antiferromagnetic interaction between the nearest neighboring Mn^{2+}.

Field-dependent magnetizations ($M(H)$) at 5 K and in the vicinity of T_C are shown in Figure 3c,d, respectively. At low

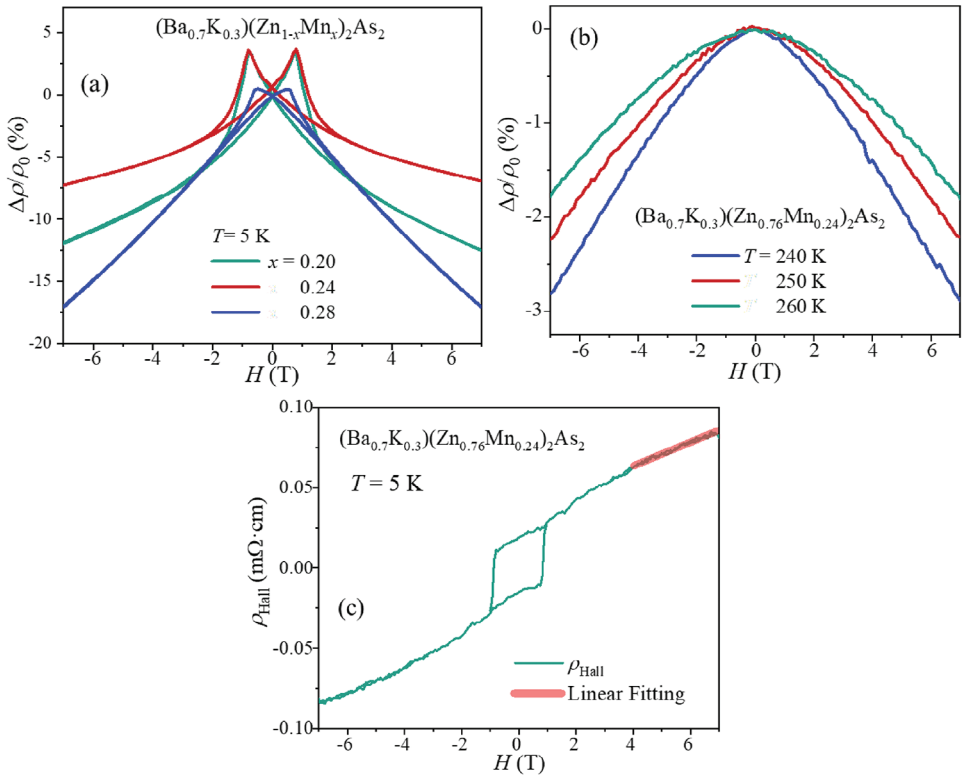

Figure 4. a) Field-dependent magnetoresistance of $(Ba_{0.7}K_{0.3})(Zn_{1-x}Mn_x)_2As_2$ with $x = 0.2$, 0.24, and 0.28 at 5 K. b) Field-dependent magnetoresistance of $(Ba_{0.7}K_{0.3})(Zn_{0.76}Mn_{0.24})_2As_2$ at 240, 250 and 260 K. c) Hall effect results of $(Ba_{0.7}K_{0.3})(Zn_{0.76}Mn_{0.24})_2As_2$ at 5 K.

temperatures, one can find robust magnetic loops with H_C of ≈0.5 T. The doping-level dependence of H_C also shows a dome-shaped relationship similar to the x dependence of T_C. The sample $(Ba_{0.7}K_{0.3})(Zn_{0.76}Mn_{0.24})_2As_2$ with the highest T_C exhibits the largest H_C of 0.8 T. The saturate magnetizations (M_S) are ≈1 μ_B/Mn consistent with lower Mn-doped samples.[9,22] In the vicinity of T_C, magnetic loops are measured to confirm the ferromagnetic ordering. At 257 K, $(Ba_{0.7}K_{0.3})(Zn_{0.76}Mn_{0.24})_2As_2$ still shows an open loop indicating the forming of ferromagnetic ordering, while the rest of the samples exhibit nearly linear loops indicating paramagnetic states.

2.3. Magnetoresistance and Hall Effect

Negative magnetoresistance (MR) is also strong evidence of ferromagnetism in DMS materials, due to the reduction in spin scattering with increasing external magnetic fields.[5,29–31] The temperature dependence of resistivity shows semiconducting behavior within the measuring temperature range (5 to 300 K). Below T_C, MR can be found for all the samples. At 5 K, butterfly-like MR(H) curves are observed, as shown in **Figure 4a**. The peaks at around 0.5 T are consistent with H_C from $M(H)$ curves. It is worth noting that the MR is far from reaching saturation at 7 T, where the magnetic moment is nearly saturated. In such conditions, the MR is presumably from the weak localization effects.[32,33] At high temperatures, negative MR is also clearly present in the vicinity of T_C, as shown in Figure 4b, evidencing the forming of ferromagnetic ordering. For the sample $(Ba_{0.7}K_{0.3})(Zn_{0.76}Mn_{0.24})_2As_2$ with T_C of 260 K, the maximum MR are −7.5% and −1.7% at 5 and 300 K, respectively. The MR with similar magnitudes have been reported in BZA with lower doping levels.[27]

To determine the carrier concentrations, Hall effect measurements were conducted. Figure 4c shows the anomalous Hall effect of $(Ba_{0.7}K_{0.3})(Zn_{0.76}Mn_{0.24})_2As_2$ at 5 K. For a ferromagnetic DMS material, the carrier scattering by the magnetic ions causes the carriers to accumulate asymmetrically in the transverse direction of the current. This scattering results in an additional contribution to the normal Hall effect, namely, the anomalous Hall effect. This is an important feature of long-range ferromagnetic ordering in a DMS material. The Hall resistance (R_{Hall}) can be phenomenologically described by Equation (1)

$$R_{Hall} = R_0 H + R_s M \tag{1}$$

where R_0 is the ordinary Hall coefficient, R_s for the anomalous one, and M for the magnetization moment.[34] At high magnetic fields, the magnetization saturates and then the anomalous Hall component R_sM becomes independent of the magnetic field. Thus, one can deduce the ordinary Hall coefficient R_0 from the high-field slope of R_{Hall}. The calculated carrier concentration $n_p = +3.9 \times 10^{20}$ cm^{-3} at 5 K, and the positive sign indicates p-type carriers. The value of carrier concentration is comparable to previous studies on lower Mn-doped BZA and classical (Ga,Mn)As.[9,22,35]

Table 1. First-principles magnetic exchange couplings of Mn—Mn pairs in $Ba(Zn_{0.75}Mn_{0.25})_2As_2$, $Ba(Zn_{0.75}Mn_{0.25})_2As_2$, $(Ba_{0.875}K_{0.125})(Zn_{0.75}Mn_{0.25})_2As_2$, $(Ba_{0.75}K_{0.25})(Zn_{0.75}Mn_{0.25})_2As_2$ and $(Ga_{0.91}Mn_{0.09})As$. J_1, J_2, J_3, and $J_\perp$ are intralayer couplings of the nearest, the next-nearest, the third-nearest neighbors and interlayer couplings respectively. Two Mn impurities are coupled ferromagnetically for conditions with $J > 0$ and antiferromagnetically for conditions with $J < 0$.

First-principles calculations				
	J_1 [meV]	J_2[meV]	J_3[meV]	$J_\perp$[meV]
$Ba(Zn_{0.75}Mn_{0.25})_2As_2(Ba_{0.875}K_{0.125})(Zn_{0.75}Mn_{0.25})_2As_2$	−8.76–5.46	−2.47–0.71	0.170.58	−1.471.15
$(Ba_{0.75}K_{0.25})(Zn_{0.75}Mn_{0.25})_2As_2$	−1.49	1.73	1.11	2.62
$(Ba_{0.5}K_{0.5})(Zn_{0.75}Mn_{0.25})_2As_2(Ga_{0.91}Mn_{0.09})As$	0.318.31	2.95–0.63	2.950.81	2.32

2.4. First-Principles Simulations

To study the magnetic interactions between Mn impurities in BZA, a Heisenberg Hamiltonian with the nearest coupling J_1, the next-nearest coupling J_2, the third-nearest neighbor couplings J_3, and the interlayer couplings $J_\perp$ of the Mn—Mn pairs is employed, as described by Equation (2),

$$H = \sum_{\langle i,j\rangle} J_1 S_i \cdot S_j + \sum_{\langle i,j\rangle} J_2 S_i \cdot S_j + \sum_{\langle\langle\langle i,j\rangle\rangle\rangle} J_3 S_i \cdot S_j + \sum_{\langle i,i'\rangle} J_\perp S_i \cdot S_{i'} \quad (2)$$

Using the density functional theory calculations, the exchange couplings J_1, J_2, J_3 and $J_\perp$ for the different supercells of $Ba(Zn_{0.75}Mn_{0.25})_2As_2$, $(Ba_{0.875}K_{0.125})(Zn_{0.75}Mn_{0.25})_2As_2$, $(Ba_{0.75}K_{0.25})(Zn_{0.75}Mn_{0.25})_2As_2$ and $(Ba_{0.5}K_{0.5})(Zn_{0.75}Mn_{0.25})_2As_2$ are calculated. Further details can be found in the Supporting Information. The results are listed in **Table 1**, with ferromagnetic for $J > 0$, and antiferromagnetic for $J < 0$.

To estimate the Néel temperature (T_N) for the antiferromagnetic cases and the T_C for the ferromagnetic cases, the following mean-field formula is used, as described by Equation (3),

$$T_{N/C} = \frac{2}{3k_B} S(S+1) \sum_i \sum_\alpha Z_i^\alpha P_\alpha J_i \quad (3)$$

where J_i (i = 1, 2, 3, ⊥) represents the above exchange couplings, Z_i^α is the coordination number of Mn impurities in one inequivalent doping configuration α for a given doping concentration, and P_α is the probability of this doping configuration. Further details can be found in the Supplemental Materials. S = 5/2 is used for the spin of the Mn impurities with five local d orbits. A rescaled method is adopted to counteract the overestimation of the mean-field result, where the calculated mean-field T_C of $(Ba_{0.75}K_{0.25})(Zn_{0.85}Mn_{0.15})_2As_2$ is approximated to correspond to T_C of 230 K of $(Ba_{0.7}K_{0.3})(Zn_{0.85}Mn_{0.15})_2As_2$ in the experiment. All mean-field T_C and T_N for $Ba(Zn_{0.75}Mn_{0.25})_2As_2$ and $(Ba_{1-y}K_y)(Zn_{1-x}Mn_x)_2As_2$ are divided by the mean-field T_C of $(Ba_{0.75}K_{0.25})(Zn_{0.75}Mn_{0.15})_2As_2$ to obtain the ratios, which are used to multiply 230 K and estimate more reliable T_C or T_N as depicted in **Figure 5**.

For comparison, the magnetic exchange couplings J_1, J_2, and J_3 and T_C of $(Ga_{1-x}Mn_x)As$ are also calculated in a similar way. The rescaled method is also adopted to counteract the overestimation of the mean-field result, where the calculated mean-field T_C of $(Ga_{0.figur84}Mn_{0.16})As$ is approximated to correspond to the T_C of 200 K of $(Ga_{0.84}Mn_{0.16})As$ in experiments.[24,36] As shown in Figure 5a, the T_C increases with increased Mn concentration for $(Ga_{1-x}Mn_x)As$ and $(Ba_{0.75}K_{0.25})(Zn_{1-x}Mn_x)_2As_2$ with x in the range of 5% to 30%. This behavior is consistent with the experimental result of $(Ba_{0.7}K_{0.3})(Zn_{1-x}Mn_x)_2As_2$. As shown in Figure 5b, $(Ba_{1-y}K_y)(Zn_{0.75}Mn_{0.15})_2As_2$ shows antiferromagnetic behavior without hole doping (namely, K doping). With the increased carrier concentration y, the antiferromagnetic coupling is suppressed and becomes ferromagnetic for y reaching 25%. For K-underdoped samples $(Ba_{0.875}K_{0.125})(Zn_{1-x}Mn_x)_2As_2$, it is antiferromagnetic coupling, and the T_N increases with increased x as depicted in Figure 5c.

3. Conclusion

The new type of diluted magnetic semiconductors $(Ba_{0.7}K_{0.3})(Zn_{1-x}Mn_x)_2As_2$ with a record high T_C are synthesized via the proper high-pressure annealing. With Mn content of 24%, we obtain the highest reliable T_C of 260 K among diluted magnetic semiconductors with independent spin and carrier doping, showing promising application potential. Moreover, first-principles calculations of magnetic interactions between nearest-neighbor Mn ions show that the antiferromagnetism can be suppressed by increasing K doping in the DMS $(Ba,K)(Zn,Mn)_2As_2$. Thus our results suggest a promising method to achieve room temperature or even higher Tc ferromagnetism for $(Ba,K)(Zn,Mn)_2As_2$ and analogs. It is noted that further K doping over 30% could not be accomplished at current synthesis conditions. Although Ba^{2+} and K^+ have similar ionic sizes, $Ba(Zn,Mn)_2As_2$ and $K(Zn,Mn)As$ crystalize into a tetragonal and a hexagonal structure, respectively.[37] Much higher synthesis pressures would be required to break the limitation of the (Ba,K) solution in $(Ba,K)(Zn,Mn)_2As_2$.

On the other hand, the DMS $(Ba,K)(Zn,Mn)_2As_2$, antiferromagnetic $BaMn_2As_2$, and superconducting $(Ba,K)Fe_2As_2$ have the identical crystal structure. In addition, there is quite good lattice matching within the *a-b* plane (mismatch <5%). This unique feature provides distinct advantages in fabricating new functional devices based on the heterojunctions of various combinations of aforementioned diluted magnetic semiconductors, superconductors, and magnetic states.[3,17,19] The near room-temperature ferromagnetism means that $(Ba,K)(Zn,Mn)_2As_2$ shows promise for the development of new spintronic devices.

4. Experimental Section

Synthesis: High-purity raw materials, including Ba, K, Zn, Mn, and As, were mixed and ground in a glove box according to the nominal molar

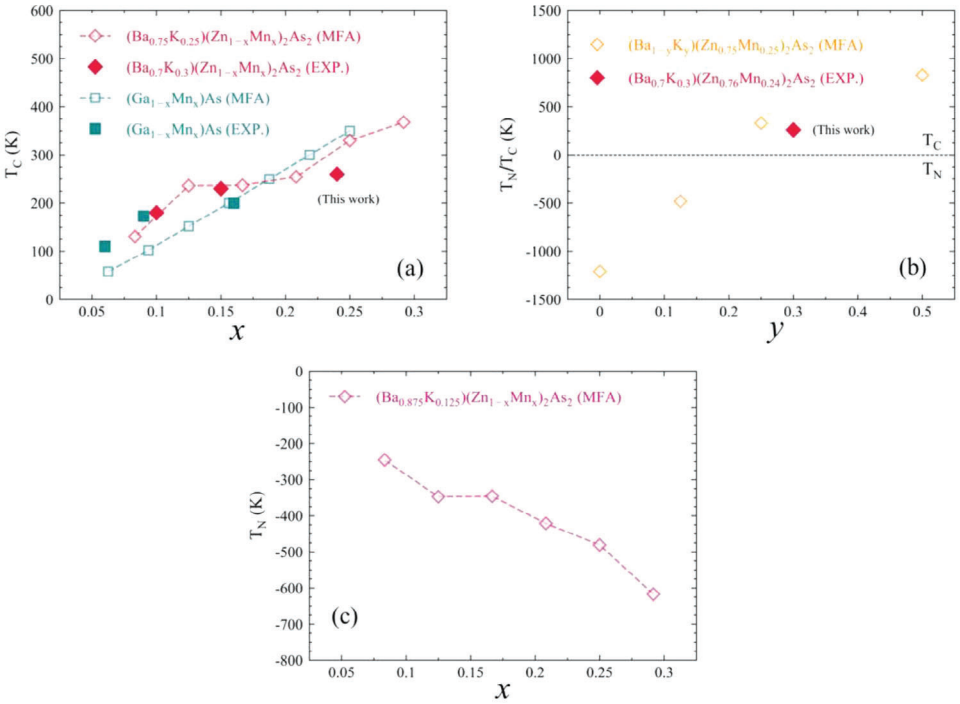

Figure 5. a) Rescaled mean-field T_C of $(Ba_{0.75}K_{0.25})(Zn_{1-x}Mn_x)_2As_2$ and $(Ga_{1-x}Mn_x)As$ versus Mn concentration. Experimental results of T_C are labeled with solid markers.[8,16,18] b) Rescaled mean-field T_N (<0) or T_C (>0) for $Ba(Zn_{0.75}Mn_{0.25})_2As_2$, $(Ba_{0.75}K_{0.25})(Zn_{0.75}Mn_{0.25})_2As_2$ and $(Ba_{0.5}K_{0.5})(Zn_{0.75}Mn_{0.25})_2As_2$. c) Rescaled mean-field T_N for $(Ba_{0.875}K_{0.125})(Zn_{1-x}Mn_x)_2As_2$.

ratio. The mixture loaded in a crucible was sealed in a Nb tube and then a quartz tube, and calcined at 950 K for 12 h. The products were then reground, and annealed under 800 K and 5.5 GPa for 1 h with a high-pressure press. Such high-pressure annealing treatment can increase the chemical solution of Zn-Mn and retain volatile elements simultaneously. It is noted that the high-pressure annealing in this work is different from the high-pressure used in the previous report.[15] For the former, the samples are fabricated via high-pressure annealing at 800 K to overcome the limitation of chemical solution in the lattice of BZA. For the latter, the samples were synthesized under ambient pressure, and then loaded into high-pressure generators, diamond anvil cells, to study the pressure effect on ferromagnetic interaction and T_C of BZA within temperature range of 2–300 K.

General Properties Characterization: Powder X-ray diffraction (XRD) was carried out for the component analysis of resulting products, using Cu-K_α radiation with a Philips X'pert diffractometer at room temperature. Energy dispersive X-ray analysis (EDX) of a commercial scanning electron microscope (SEM) was used for the confirmation of chemical compositions of polycrystal specimens. The real doping ratio is consistent with nominal composition. For the sake of simplification, the nominal formulas are used in the following text. Characterization of *dc* magnetic susceptibility for all the samples was accomplished by superconducting quantum interference device (SQUID). Electricity transport measurements were conducted via a physical property measurement system (PPMS).

First-Principles Calculations: First-principles simulations were performed with the projector augmented wave (PAW) method using the Vienna ab Initio simulation package (VASP).[38,39] The choice of the electron exchange-correlation functional was generalized gradient approximation (GGA) with the form of Perdew-Burke-Ernzerhof (PBE) realization.[40] The GGA plus on-site Coulomb repulsion U (GGA + U) approach by Dudarev et al. was used to describe strongly localized Mn 3d orbitals.[41] The effective on-site Coulomb interaction parameter (U = 4 eV) was applied to Mn 3d orbitals. Lattice constants and atomic positions were fully relaxed until the maximum force acting on all atoms was less than 1×10^{-3} eV and the total energy was converged to 1×10^{-7} eV with the Gaussian smearing method. The kinetic energy cutoff of 450 eV was employed. The Brillouin zone was sampled with a $4 \times 4 \times 8$ Monkhorst–Pack grid for calculations of magnetic exchange couplings with $2 \times 2 \times 1$ supercells of $(Ba_{1-y}K_y)(Zn_{1-x}Mn_x)_2As_2$.[42] All doping configurations with corresponding doping probabilities are generated by disorder code.[43,44]

Supporting Information

Supporting Information is available from the Wiley Online Library or from the author.

Acknowledgements

The work was supported by the National Key R&D Program of China (No. 2022YFA1403900), and the CAS Project for Young Scientists in Basic Research (No. YSBR-030). Z.D. acknowledges support of the Youth Innovation Promotion Association of CAS (No. 2020007). B.G. is supported by the National Natural Science Foundation of China (No. 12074378), Chinese Academy of Sciences (No. JZHKYPT-2021-08 and No. XDB33000000). Y.P. and X.L. contributed equally to this work.

Conflict of Interest

The authors declare no conflict of interest.

Data Availability Statement

The data that support the findings of this study are available from the corresponding author upon reasonable request.

Keywords

diluted magnetic semiconductors, high Curie temperature, independent spin and carrier doping

Received: August 30, 2024
Revised: October 3, 2024
Published online: November 22, 2024

[1] I. Žutić, J. Fabian, S. D. Sarma, *Rev. Mod. Phys.* **2004**, *76*, 323.
[2] M. Jiang, H. Asahara, S. Ohya, *Adv. Sci.* **2023**, *10*, 2301540.
[3] A. Hirohata, H. Sukegawa, H. Yanagihara, I. Zutic, T. Seki, S. Mizukami, R. Swaminathan, *IEEE Trans. Magn.* **2015**, *51*, 1.
[4] A. Chernyshov, M. Overby, X. Liu, J. K. Furdyna, Y. Lyanda-Geller, L. P. Rokhinson, *Nat. Phys.* **2009**, *5*, 656.
[5] X. Liu, L. Riney, J. Guerra, W. Powers, J. Wang, J. K. Furdyna, B. A. Assaf, *J. Semicond.* **2022**, *43*, 112502.
[6] Z. Deng, C. Q. Jin, Q. Q. Liu, X. C. Wang, J. L. Zhu, S. M. Feng, L. C. Chen, R. C. Yu, C. Arguello, T. Goko, F. Ning, J. Zhang, Y. Wang, A. A. Aczel, T. Munsie, T. J. Williams, G. M. Luke, T. Kakeshita, S. Uchida, W. Higemoto, T. U. Ito, B. Gu, S. Maekawa, G. D. Morris, Y. J. Uemura, *Nat. Commun.* **2011**, *2*, 422.
[7] N. T. Tu, P. N. Hai, L. D. Anh, M. Tanaka, *Appl. Phys. Express* **2019**, *12*, 103004.
[8] J. K. Glasbrenner, I. Zutic, I. I. Mazin, *Phys. Rev. B* **2014**, *90*, 140403(R).
[9] Z. Deng, K. Zhao, B. Gu, W. Han, J. L. Zhu, X. C. Wang, X. Li, Q. Q. Liu, R. C. Yu, T. Goko, B. Frandsen, L. Liu, J. Zhang, Y. Wang, F. L. Ning, S. Maekawa, Y. J. Uemura, C. Q. Jin, *Phys. Rev. B* **2013**, *88*, 081203(R).
[10] K. Zhao, Z. Deng, X. C. Wang, W. Han, J. L. Zhu, X. Li, Q. Q. Liu, R. C. Yu, T. Goko, B. Frandsen, L. Liu, F. Ning, Y. J. Uemura, H. Dabkowska, G. M. Luke, H. Luetkens, E. Morenzoni, S. R. Dunsiger, A. Senyshyn, P. Böni, C. Q. Jin, *Nat. Commun.* **2013**, *4*, 1442.
[11] H. Suzuki, K. Zhao, G. Shibata, Y. Takahashi, S. Sakamoto, K. Yoshimatsu, B. J. Chen, H. Kumigashira, F.-H. Chang, H.-J. Lin, D. J. Huang, C. T. Chen, B.o Gu, S. Maekawa, Y. J. Uemura, C. Q. Jin, A. Fujimori, *Phys. Rev. B* **2015**, *91*, 140401(R).
[12] B. J. Chen, K. Zhao, Z. Deng, W. Han, J. L. Zhu, X. C. Wang, Q. Q. Liu, B. Frandsen, L. Liu, S. Cheung, F. L. Ning, T. J. S. Munsie, T. Medina, G. M. Luke, J. P. Carlo, J. Munevar, Y. J. Uemura, C. Q. Jin, *Phys. Rev. B* **2014**, *90*, 155202.
[13] J. Masek, J. Kudrnovský, F. Máca, B. L. Gallagher, R. P. Campion, D. H. Gregory, T. Jungwirth, *Phys. Rev. Lett.* **2007**, *98*, 067202.
[14] I. Žutić, T. Zhou, *Sci. China. Phys. Mech.* **2018**, *61*, 067031.
[15] F. Sun, N. N. Li, B. J. Chen, Y. T. Jia, L. J. Zhang, W. M. Li, G. Q. Zhao, L. Y. Xing, G. Fabbris, Y. G. Wang, Z. Deng, Y. J. Uemura, H. K. Mao, D. Haskel, W. G. Yang, C. Q. Jin, *Phys. Rev. B* **2016**, *93*, 224403.
[16] T. Dietl, H. Ohno, *Rev. Mod. Phys.* **2014**, *86*, 187.
[17] I. Žutić, S. D. Sarma, *Phys. Rev. B* **1999**, *60*, R16322.
[18] R. Cai, Y. Yao, P. Lv, Y. Ma, W. Xing, B. Li, Y. Ji, H. Zhou, C. Shen, S. Jia, X. C. Xie, I. Žutić, Q.-F. Sun, W. Han, *Nat. Commun.* **2021**, *12*, 6725.
[19] I. Zutic, A. Matos-Abiague, B. Scharf, H. Dery, K. Belashchenko, *Mater. Today* **2019**, *22*, 85.
[20] B. A. Frandsen, Z. Gong, M. W. Terban, S. Banerjee, B. Chen, C. Jin, M. Feygenson, Y. J. Uemura, S. J. L. Billinge, *Phys. Rev. B* **2016**, *94*, 094102.
[21] M. A. Surmach, B. J. Chen, Z. Deng, C. Q. Jin, J. K. Glasbrenner, I. I. Mazin, A. Ivanov, D. S. Inosov, *Phys. Rev. B* **2018**, *97*, 104418.
[22] F. Sun, G. Q. Zhao, C. A. Escanhoela, B. J. Chen, R. H. Kou, Y. G. Wang, Y. M. Xiao, P. Chow, H. K. Mao, D. Haskel, W. G. Yang, C. Q. Jin, *Phys. Rev. B* **2017**, *95*, 094412.
[23] S. Yu, G. Zhao, Y.i Peng, X. Zhu, X. Wang, J. Zhao, L. Cao, W. Li, Z. Li, Z. Deng, C. Jin, *APL Mater.* **2019**, *7*, 101119.
[24] L. Chen, X. Yang, F. Yang, J. Zhao, J. Misuraca, P. Xiong, S. von Molnár, *Nano Lett.* **2011**, *11*, 2584.
[25] Q. Wei, H. Wang, X. Zhao, J. Zhao, *J. Semicond.* **2022**, *43*, 072101.
[26] M. Tanaka, *Jpn. J. Appl. Phys.* **2021**, *60*, 010101.
[27] K. Zhao, B. Chen, G. Zhao, Z. Yuan, Q. Liu, Z. Deng, J. Zhu, C. Jin, *Chin. Sci. Bull.* **2014**, *59*, 2524.
[28] Z. Deng, X. Wang, M. Wang, F. Shen, J. Zhang, Y. Chen, H. L. Feng, J. Xu, Y. Peng, W. Li, J. Zhao, X. Wang, M. Valvidares, S. Francoual, O. Leupold, Z. Hu, L. H. Tjeng, M.-R. Li, M. Croft, Y. Zhang, E. Liu, L. He, F. Hu, J. Sun, M. Greenblatt, C. Jin, *Adv. Mater.* **2023**, *35*, 2209759.
[29] F. Matsukura, M. Sawicki, T. Dietl, D. Chiba, H. Ohno, *Phys. E* **2004**, *21*, 1032.
[30] S. Dong, L. Riney, X. Liu, *Phys. Rev. Mater.* **2021**, *5*, 014402.
[31] M. Csontos, G. Mihály, B. Jankó, T. Wojtowicz, X. Liu, J. K. Furdyna, *Nat. Mater.* **2005**, *4*, 447.
[32] G. Q. Zhao, C. J. Lin, Z. Deng, G. X. Gu, S. Yu, X. C. Wang, Z. Z. Gong, Y. J. Uemura, Y. Q. Li, C. Q. Jin, *Sci. Rep.* **2017**, *7*, 14473.
[33] N. Nagaosa, J. Sinova, S. Onoda, A. H. MacDonald, N. P. Ong, *Rev. Mod. Phys.* **2010**, *82*, 1539.
[34] H. Wang, S. Sun, J. Lu, J. Xu, X. Lv, Y. Peng, X.i Zhang, Y. Wang, G. Xiang, *Adv. Funct. Mater.* **2020**, *30*, 2002513.
[35] H. Ohno, *J. Magn. Magn. Mater.* **1999**, *200*, 110.
[36] X. Li, J.-W. Li, J.-Y. You, *et al.*, *Arxiv* **2024**, 2311.
[37] R. Vogel, H.-U. Schuster, *Z. Naturforsch B* **1980**, *35*, 114.
[38] P. E. Blochl, *Phys. Rev. B* **1994**, *50*, 17953.
[39] G. Kresse, J. Furthmuller, *Phys. Rev. B* **1996**, *54*, 11169.
[40] J. P. Perdew, K. Burke, M. Ernzerhof, *Phys. Rev. Lett.* **1996**, *77*, 3865.
[41] H. J. Monkhorst, J. D. Pack, *Phys. Rev. B* **1976**, *13*, 5188.
[42] S. L. Dudarev, G. A. Botton, S. Y. Savrasov, C. J. Humphreys, A. P. Sutton, *Phys. Rev. B* **1998**, *57*, 1505.
[43] J.-C. Lian, H.-Y. Wu, W.-Q. Huang, W. Hu, G.-F. Huang, *Phys. Rev. B* **2020**, *102*, 134209.
[44] J.-C. Lian, Y. Si, T. Huang, W.-Q. Huang, W. Hu, G.-F. Huang, *Phys. Rev. B* **2022**, *105*, 014201.